Int j simul model 24 (2025) 4, 683-693
Original scientific paper

CFD-BASED OPTIMIZATION OF BOX-TYPE AFTERTREATMENT SYSTEMS

Abdalla, A.
School of Intelligent Network and New Energy Vehicle, Geely University of China, Chengdu, P.R. China
E-Mail: anisehabdalla@guc.edu.cn

Abstract
Meeting stringent emission requirements for heavy-duty diesel engines necessitates advanced aftertreatment systems with efficient, compact packaging. This study utilizes a computational fluid dynamics (CFD) tool to optimize box-type aftertreatment system in an integrated and compact formulation. The limited available space for flow mixing poses a challenge for achieving flow uniformity within the aftertreatment system, necessitating optimization of the packaging. Various design configurations are explored through simulation optimizations. The reliable CFD models were verified with good prediction accuracy for pressure drop, soot accumulation, and temperature distribution during diesel particulate filter (DPF) loading and regeneration processes. Optimized inlet configurations with strategic mixer placement achieved a flow uniformity index from 0.788 to 0.857, improving the system performance by 8.8 %. The results offer important insights for aftertreatment system design to meet emission regulations while maintaining compact packaging requirements.
(Received in July 2025, accepted in September 2025. This paper was with the author 2 weeks for 2 revisions.)

Key Words: CFD Simulation, Aftertreatment System, Flow Uniformity, Emission Control, Box-Type Packaging

1. INTRODUCTION

The increasing number of vehicles in the world and the consequent development of the transportation structure, especially in urban areas, is one of the major causes of atmospheric pollution around the world. The diesel engine produces a broad range of atmospheric pollutant emissions during the combustion of diesel fuel in the vehicle, requiring the development of a variety of post-combustion Emission Control Technologies (ECTs) [1, 2]. It is clear that harmful emissions are likely to increase at the same rate as increasing vehicle sales unless effective mitigating policies are implemented [3]. It is important to adopt stringent emission regulations such as China VI, Euro VI, and US 2010 diesel engine standards for solving this environmental challenge [4-7]. PM and NO_x are the most pollutants produced from heavy-duty (HD) vehicles amongst other automotive system types [8]. The solution is to introduce tight aftertreatment systems made of diesel oxidation catalysts (DOC), catalysed diesel particulate filters (DPF), and selective catalytic reduction (SCR) components. The move from traditional inline aftertreatment layouts to compact box-type packaging is an important, previously non-existing, aspect in terms of system design philosophy due to the space constraints becoming more restrictive for modern heavy duty truck vehicles [9]. Box-type aftertreatment systems provide critical packaging advantages that can deliver the large volume reduction necessary for vehicle integration while maintaining all required emission control functionality. However, during the transition towards integrated compact systems, various difficult technical problems will significantly influence the performance of the system. The lack of space for elaborate exhaust gas flow mixing presents significant challenges for obtaining good exhaust gas flow uniformity in the aftertreatment system, which directly impacts emission conversion efficiency and catalyst durability [10-12]. With conventional inline configurations, there is enough space between parts to allow time to develop flow and to allow for mixing. Box-type systems, on the other hand, reduce these distances and induce complex flow structures that can lead to non-uniform velocity, temperature, and species distributions at the entrance of at least some components [13]. Adoption of aftertreatment technologies, such as diesel particulate filters (DPFs), has become imperative for controlling PM accumulation [14]. The majority of the literature to date has not addressed the integrated DOC-DPF-SCR system performance, but only the optimization of single component. Belot et al. [15] achieved large performances improvements in the individual component modelling, but there are few works at a system level that take into account the component couplings that arise in compact packaging. Most of the current studies focuses on the conventional inline schemes, while limited attention has been paid to distinct flow features and optimization implemented in the box-type packaging configuration [16, 17]. Although DPF regeneration kinetics and mixing enhancement techniques have been the subject of separate studies, no comprehensive methodologies are currently available that take into account both flow uniformity optimisation and emission performance. Previous studies have investigated soot combustion efficiency in aftertreatment components [18]. However, little knowledge exists yet regarding methods for obtaining optimal flow distribution in compact aftertreatment systems. It is essential to study the relation between flow uniformity and catalyst performance in restricted spaces since the catalytic activity is significantly related to the flow distribution [19-21]. Despite the progress in numerical simulation, few numerical studies in the literature have rigorous experimental validation, such as for complex multi-component systems operating under realistic transient conditions. Despite the progress made in the development of CFD modelling capability, experimental validation with extensive datasets, including loading and regeneration process is limited [22, 23]. This study fills this gap by creating an in depth CFD based optimization framework specifically designed for box-type aftertreatment. This study presents some unprecedented findings on the optimization of aftertreatment system. First, it provides the most complete validation of coupled 1D/3D CFD models for integrated DOC-DPF-SCR systems available in the literature that has been performed against an extended experimental datasets covering a variety of operating conditions and transient scenarios. Secondly, it develops a systematic approach to optimize flow uniformity in box-type package, with quantitative measures and design guideline that were absent in the literature. Third, it provides the first systematic study of the interactions of components in a compact package, targeting system level optimization, instead of component level performance. Finally, it translates technical numerical results into practical guidelines for the design recommendations, thus reducing the divide between academia and industry.

2. METHODOLOGY

2.1 Numerical modelling approach

The simulation framework employs both 1D and 3D computational fluid dynamics models implemented in AVL BOOST and AVL FIRE software packages. Advanced simulation modelling has demonstrated the effectiveness of computational approaches for optimizing vehicle emission reduction systems [24], providing a foundation for the integrated system optimization approach employed in this study. The 1D models facilitate parameter calibration and validation against experimental data, while 3D models provide detailed spatial analysis of flow uniformity and thermal distribution. To simulate the box-type packaging in the baseline model of the aftertreatment system, we employed a more detailed approach, utilizing a mesh consisting of 1.26 million cells, as depicted in Fig. 1.

The predictive modelling of compressible multicomponent gas behaviour involves solving the Reynolds-average governing equations for mass conservation, momentum, and energy. Specifically addressing gas mixture distribution problems, it is crucial that the solution of these governing equations is in a transient form.

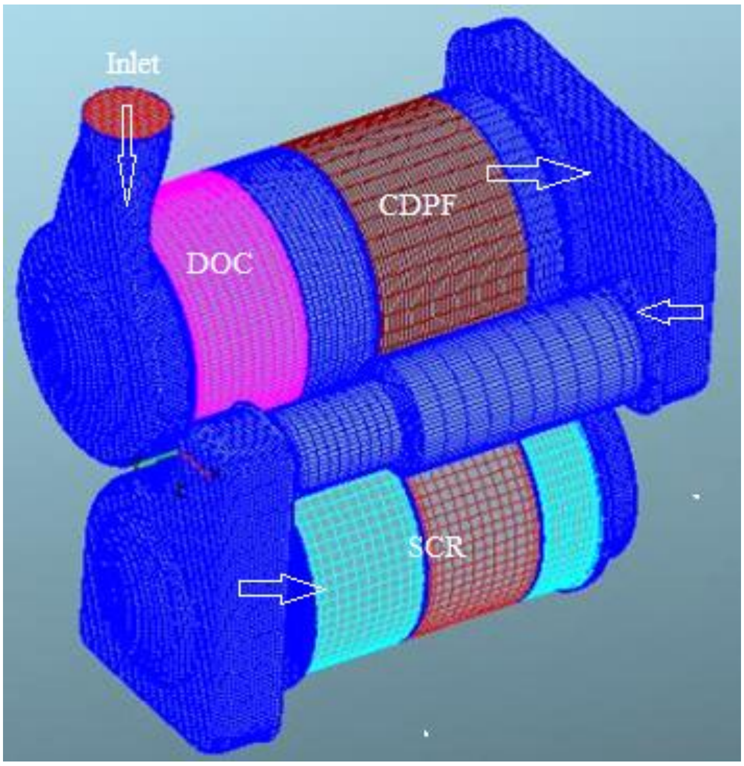

Figure 1: A computational model predicting the box-type packaging in the baseline model of the aftertreatment system.

Consequently, this study employs the unsteady average Navier-Stokes equations. The computational process commences with 3D transient simulations. The fluid properties of the multicomponent gas, including temperature, pressure, and velocity, are determined through the solution of transport equations. Notably, the injection of hydrocarbons (HC) occurs through a nozzle with a 0.5 mm diameter injector hole, delivering the HC as a spray. The injected diesel fuel is treated as a vapor phase in these simulations. To characterize the flow uniformity within the box-type aftertreatment system, we modelled the flow inside the substrates as porous media, with an enforcement of laminar flow. The turbulence effects were described by a hybrid heat transfer model approach relies on the k-ζ-f turbulence model. The models for soot loading and regeneration were constructed using AVL FIRE code. The simulation involves predicting the variation in soot mass within both the cake and depth layers, and the results are validated against experimental data.

2.2 Experimental validation setup

Validation experiments were conducted using a Dongfeng commercial diesel engine X7 with a 4-stroke, 6-cylinder configuration. The test bench includes emission measurement equipment, dynamometer, and DOC-DPF aftertreatment system with differential pressure sensors and K-type thermocouples for temperature monitoring. Soot loading in the DPF was accelerated with using the commercial Printex U (produced by Degussa). The soot loading and loading rate were controlled by the dosing pump. HD diesel engine and DOC-DPF-SCR aftertreatment system test bench conducted at Tsinghua University is shown in Fig. 2. 1D model is used for the calibration of the main parameters, such as pressure drop, temperature field and chemical reactions during loading and regeneration. The specifications of DOC and DPF which are used as the input data for the comparison are listed in Table I.

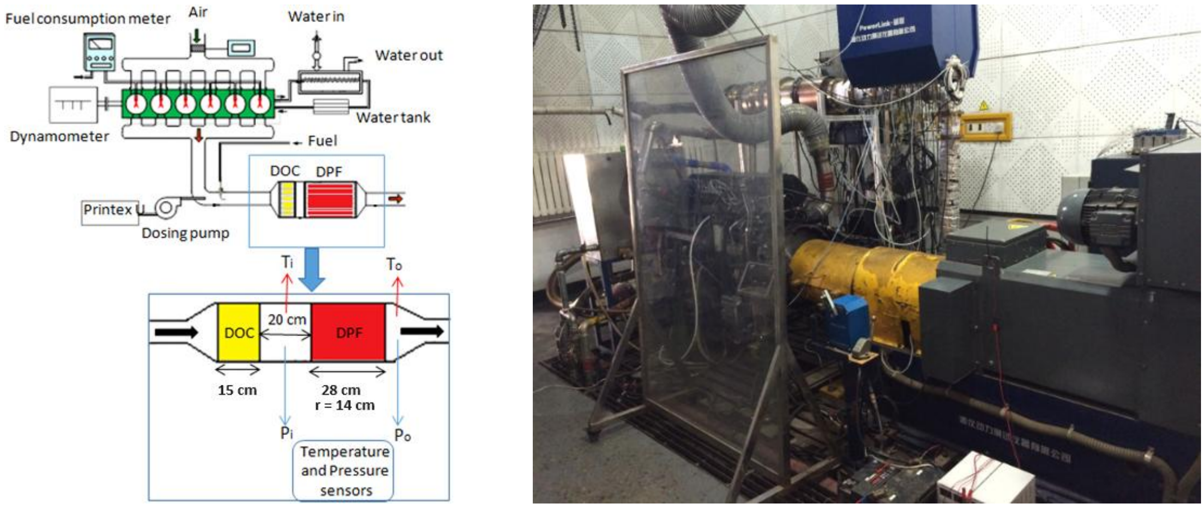

i) ii)

Figure 2: i) Diagram of the experimental setup of the engine bench with DOC-DPF system, ii) HD diesel engine and DOC-DPF-SCR aftertreatment system test bench conducted at Tsinghua University.

Table I: Properties of DOC and DPF.

DOC	
Filter type	Cordierite
Length and Diameter	15 cm × 28 cm
Filter wall thickness	0.4 mm
Cell density	400 cpsi
DPF	
Filter type	Cordierite
Length and Diameter	28 cm × 28 cm
Filter wall thickness	0.4 mm
Cell density	200 cpsi
Bulk density of DPF	1700 kg/m^3
Permeability of clean DPF	5×10^{-10} m^2
Exhaust gas inlet temperature for clean DPF	The source is measured data as shown in Fig. 3 i
Exhaust gas flow rate for clean DPF	520 kg/h
Permeability of soot layer	3.5×10^{-14} m^2
Packing density of soot	100 kg/m^3

2.3 Flow uniformity assessment

A significant obstacle in box-type packaging designs pertains to suboptimal flow uniformity. Within the confined space of the aftertreatment system in such configurations, inadequate mixing of flow occurs. Consequently, the flow uniformity index, a recognized metric for assessing flow distribution in aftertreatment contexts, is calculated at the entry points of the DOC, DPF, and SCR systems. Achieving uniform flow distribution within the box-type packaging aftertreatment system is critical for enhancing its overall operational efficiency. Flow uniformity is quantitatively assessed via the uniformity index γ, which is defined as follows:

$$\gamma_\varphi = 1 - \frac{1}{2}\frac{\int|\varphi-\overline{\varphi}|dA}{\overline{\varphi}A} \cong 1 - \frac{1}{2}\frac{\sum_{i=1}^{N}|\varphi-\overline{\varphi}|A_i}{\overline{\varphi}\sum_{i=1}^{N}A_i} \quad (1)$$

$$\bar{\varphi} = \frac{\int \varphi dA}{A} \cong \sum_{i=1}^{N} \varphi_i A_i / \sum_{i=1}^{N} A_i \tag{2}$$

where φ represents flow velocity, A is the cross-sectional area, and $\bar{\varphi}$ is the area-averaged velocity. Values range from 0 (completely non-uniform) to 1 (perfectly uniform).

3. RESULTS AND DISCUSSION

3.1 Model validation

The transient overall pressure drop for the clean DPF is simulated with an initial mass flow rate of 520 kg/h and an initial temperature curve, as depicted in Fig. 3. The input data used in the simulation are derived from measurements conducted during experimental tests. To validate the 3D numerical model, the pressure drop, soot mass amount, and temperature fields during the regeneration process are compared with both the 1D model and experimental data. Fig. 4 illustrates the comparison of 1D and 3D simulation results with measured data during a controlled regeneration for: i) pressure drop, ii) soot amount, and iii) DPF outlet temperature. The validation of 1D and 3D simulation results, encompassing pressure drop along the DPF, soot amount, and gas temperature at the DPF outlet during regeneration, reveals good and expected agreements with the experimental measured data.

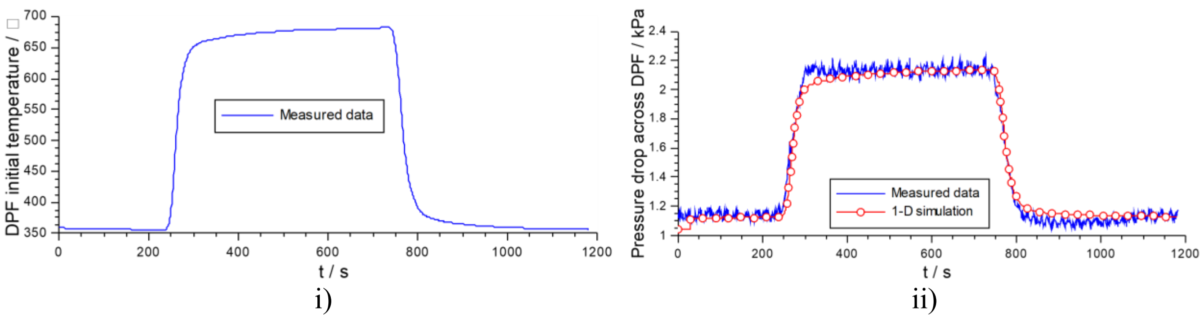

Figure 3: i) DPF inlet temperature measured data during the heating process of a clean DPF,
ii) Comparison of pressure drop across DPF between 1D simulation and experimentally measured data for a clean DPF.

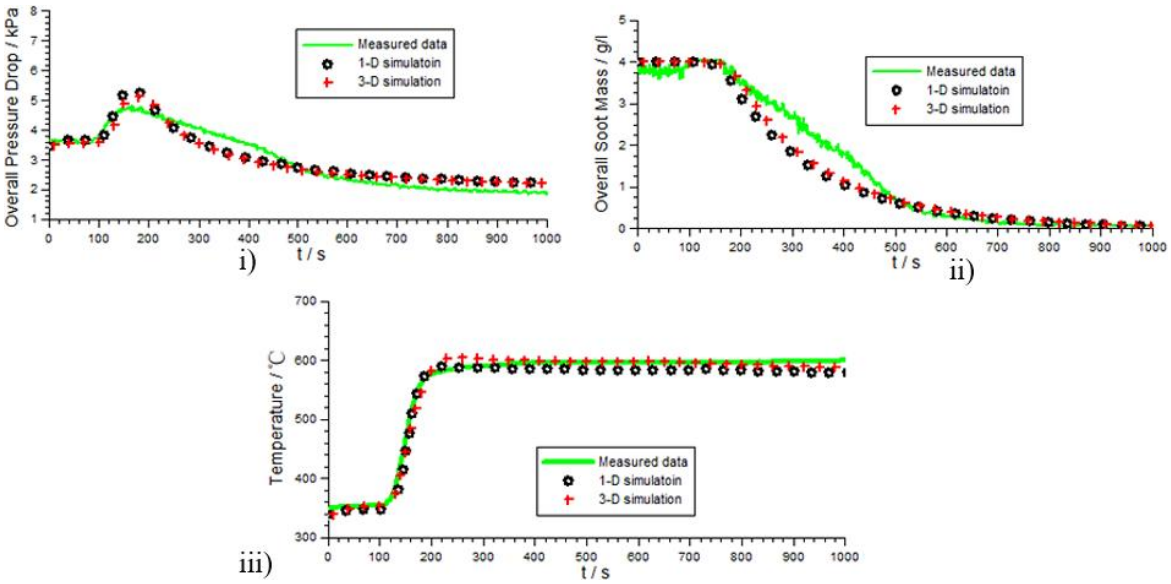

Figure 4: Comparison of 1D and 3D simulation results with measured data during a controlled regeneration encompasses; i) pressure drop, ii) soot amount, iii) DPF outlet temperature.

3.2 Flow uniformity optimization

A sensitivity analysis was conducted to explore different inlet configurations, with a focus on evaluating and comparing flow uniformity within each design. This analysis aimed to assess the impact of varying inlet conditions on the development and optimization of the box-type aftertreatment geometry, under two distinct mass flow rate conditions: low (250 kg/h at 300 °C) and high (1400 kg/h at 540 °C). The flow uniformity index, denoted as γ, was computed for each case using Eqs. (1) and (2).

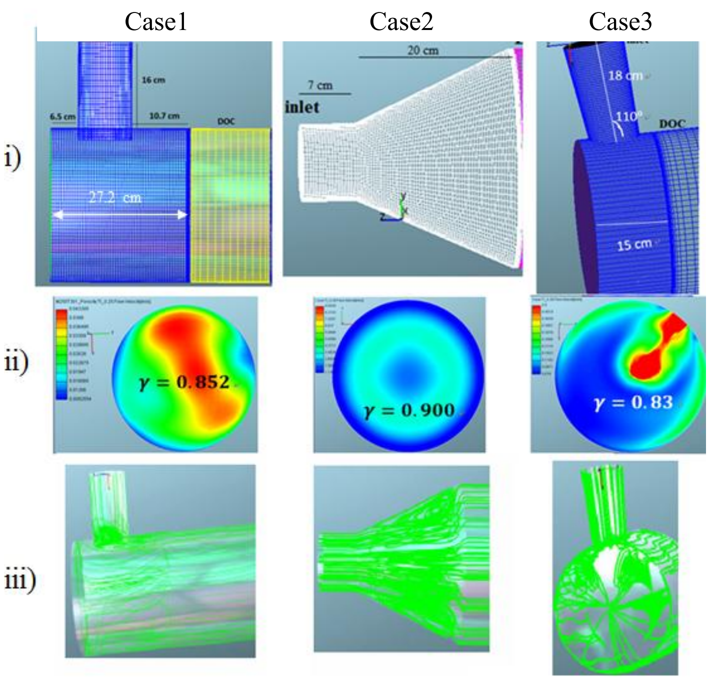

Figure 5: i) Comparison between the three inlets optimized configuration; ii) Velocity profile on the cross-section area in the entrance of DOC with velocity uniformity index values for the optimized designs is compared; iii) Gas flow streamlines are compared, the low mass flow rate is used in the simulation.

Fig. 5 i compares the three inlets optimized configuration for Case1, Case2, and Case3. Fig. 5 ii shows the velocity profile on the cross-section area in the entrance of DOC with velocity uniformity index values for the optimized designs is compared. Gas flow streamlines are also compared for each design as shown in Fig. 5 iii.

Velocity profile on the cross-section area at the entrance of DOC for the three cases (Case1, Case2, and Case3) show that Case2 has the highest flow uniformity with $\gamma = 0.9$. Due to size constraints in packaging the box-aftertreatment system on a heavy-duty diesel engine-equipped vehicle, it is necessary to shorten the distance of the tube upstream of the DOC. Hence the inlet tube length upstream of DOC for the optimized design Case2 was 27 cm. Therefore, inlet tube length upstream of DOC for Case4 is reduced to 6 cm, as shown in Fig. 6.

Fig. 6 shows the baseline case of the shortest length inlet configuration used for the optimization of a box-aftertreatment design. The flow uniformity index of Case4 is 0.788, the design of the baseline case (Case4) needs to be optimized by improving flow uniformity. The flow velocity profile on the cross-section area in front of the DOC is shown in Fig. 6 i. Higher flow velocity is observed near the centre area and the lower part of the DOC entrance. Velocity uniformity at the entrance of DOC is very low due to the bend in the inlet configuration of baseline design, the flow separates upstream of DOC and creates large vortices in the two sides upstream of DOC as shown in Fig. 6 ii.

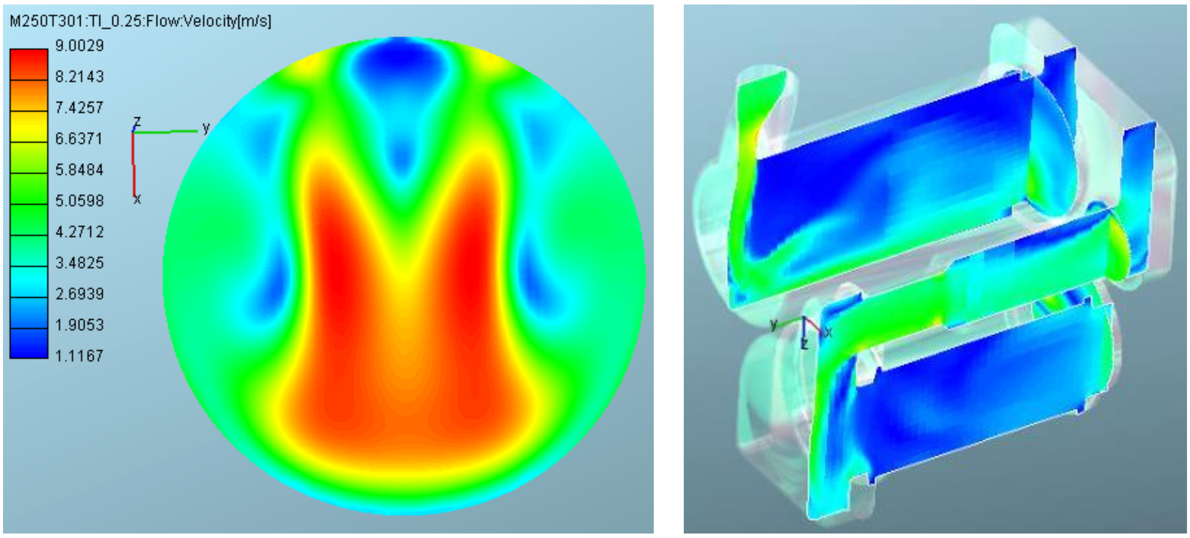

i) ii)

Figure 6: i) The velocity profile in the front of DOC for Case4, flow uniformity index γ is 0.788 (low flow condition is used in the simulation: 250 kg/h and 300 °C); ii) Velocity distribution along with the box-type packaging base model (Case4), high mass flow rate (1400 kg/h with 540 °C) is used in the simulation.

Fig. 7 presents contour plots of flow velocity and flow uniformity indices at the entrances of DOC, DPF, and SCR. In the case of baseline configuration (Case4), the flow uniformity is not good enough. Here most of the fluid flows through the centre and lower part of the catalyst, causing a higher temperature at these regions, while lower gas flows by the boundary area where heat transfer is active.

Flow and thermal uniformity upstream of DOC, DPF, and SCR are crucial in improving the performance of an aftertreatment system. The uniformity of flow could have a significant impact on emission conversion and catalyst ageing. Therefore, the aftertreatment system must be designed well to perform well across a wide range of exhaust mass flow conditions.

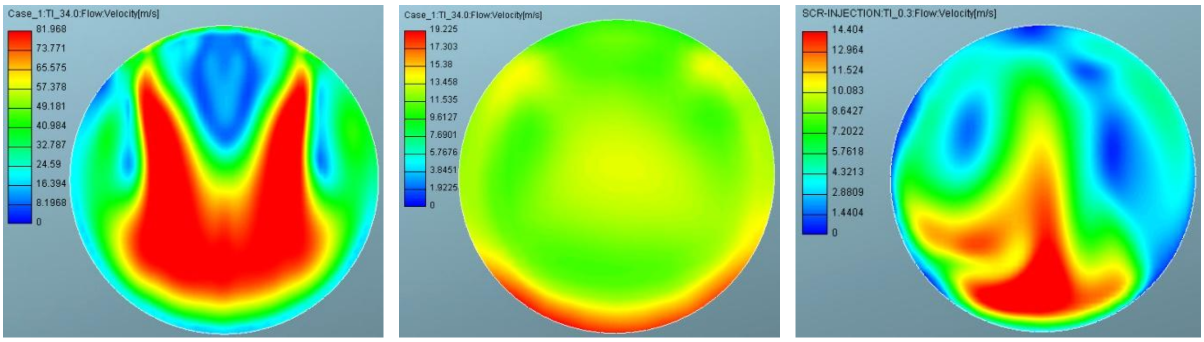

DOC_inlet $\gamma = 0.788$ DPF_inlet $\gamma = 0.99$ SCR_inlet $\gamma = 0.76$

Figure 7: Velocity profile and flow uniformity index on the cross-section areas of DOC_inlet, DPF_inlet and SCR_inlet for the baseline design without mixer (Case4), high mass flow rate (1400 kg/h with 540 °C) is used in the simulation.

As we mentioned before, flow uniformity at the entrance of DOC is very important. Hence, high uniformity at the exhaust gas improves the aftertreatment performance. Uniformity of flow at the entrance of DOC investigated under three different inlet configuration design. The three inlet configuration design are:

1. Baseline configuration without a mixer, Case4,
2. Configuration with one mixer placed upstream of DOC, Case5,

3. Configuration with three mixers placed upstream of DOC, Case6.

For Case5, a mixer is placed upstream of DOC, and downstream of inlet tube bend. Fig. 8 i shows Case5, the baseline configuration with mixer placed upstream of DOC. Fig. 8 ii shows the velocity profile at the entrance of DOC with mixer design geometry, where a high mass flow rate is used in the simulation. Flow uniformity index value upstream of DOC for the mixer design geometry (Case5) with a high mass flow rate case was 0.857. The mixer placed upstream of DOC was improved flow uniformity by 8.8 % increase in velocity uniformity index compared to baseline design (Case4).

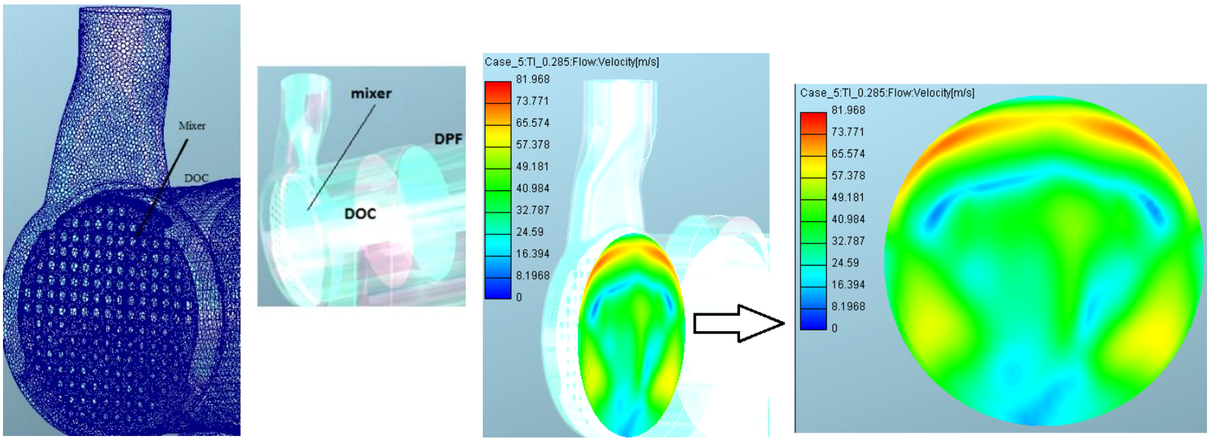

Figure 8: i) The geometry of inlet configuration with one mixer placed upstream of DOC (Case5); ii) Velocity profile of DOC_inlet for the mixer design (Case5), high mass flow rate (1400 kg/h with 540 °C) is used in the simulation. The velocity uniformity index value upstream of DOC was 0.857.

For Case6, three mixers placed upstream of DOC. Fig. 9 i shows Case6, the baseline design with three mixers placed upstream of DOC. The flow uniformity index for the three mixers design (Case6) was 0.824. Fig. 9 ii shows the flow velocity distribution at the entrance of DOC for Case6, high mass flow rate is used in the simulation.

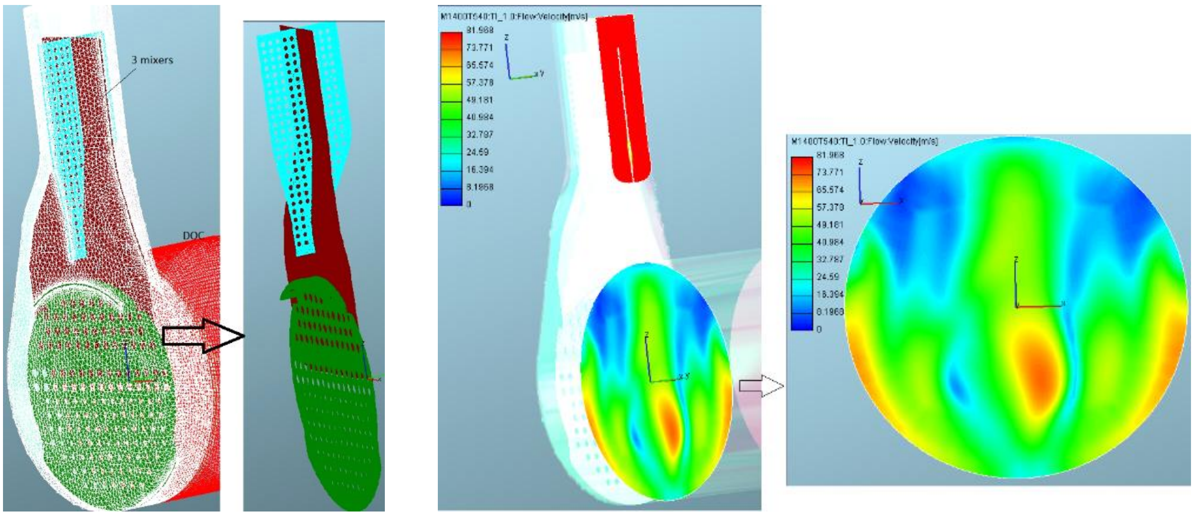

Figure 9: i) The geometry of inlet configuration with three mixers placed upstream of DOC (Case6); ii) Velocity profile of DOC inlet for the three mixers design (Case6), high mass flow rate (1400 kg/h with 540 °C) is used in the simulation. The velocity uniformity index value upstream of DOC was 0.824.

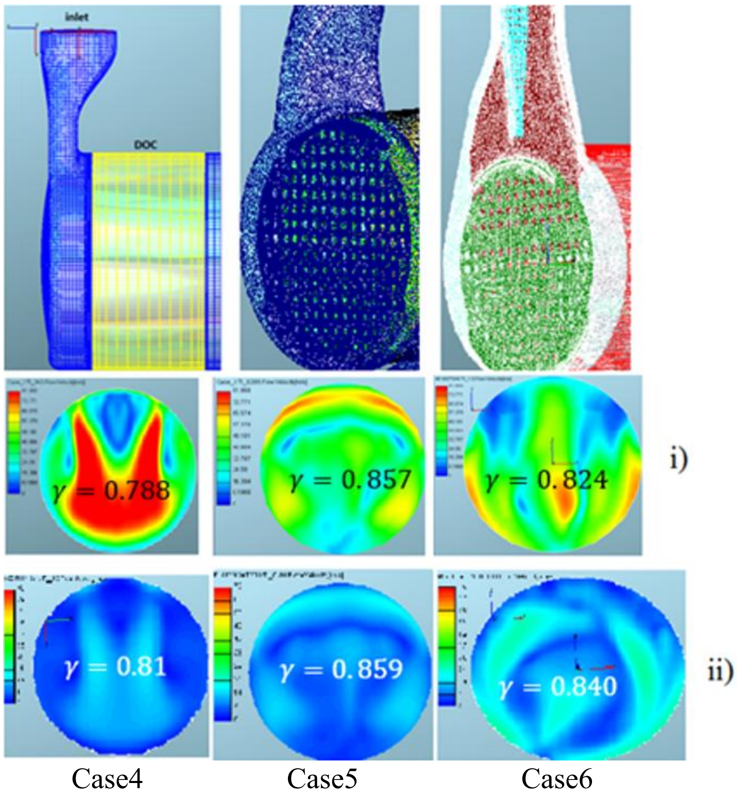

Figure 10: Comparison between velocity uniformity indexes values for the geometry design with and without a mixer; i) High mass flow rate (1400 kg/h at 540 °C) is used in the simulation; ii) Low mass flow rate (250 kg/h at 300 °C) is used in the simulation.

Fig. 10 shows the comparison between the flow uniformity for the three inlet configurations (Case4, Case5, and Case6) at low and high mass flow rates. We observed that the mixer has a large influence on flow uniformity. Highest flow uniformity index value is observed for the geometry with one mixer (Case5 as shown in Fig. 8). Simulation results depict higher uniformity for lower mass flow rate, see Fig. 10. Six different inlet configurations were evaluated. The baseline configuration (Case 4) exhibited poor flow uniformity with $\gamma = 0.788$. Strategic placement of a single mixer upstream of the DOC (Case 5) improved uniformity to $\gamma = 0.857$, representing an 8.8 % enhancement. Configurations with multiple mixers showed diminishing returns, highlighting the importance of optimal mixer design rather than quantity.

4. CONCLUSION

This study conducted a numerical investigation into flow uniformity for various inlet configurations preceding a DOC. The optimization of the inlet configuration proved instrumental in improving flow uniformity, a factor that influences the efficacy of the box-type packaging aftertreatment system. Our observations highlighted the substantial influence of the mixers. Strategic inlet configuration optimization improved flow uniformity by up to 8.8 %, with single mixer designs outperforming multiple mixer configurations. The optimized inlet configuration not only improved DOC entrance uniformity but also enhanced downstream DPF ($\gamma = 0.99$) and SCR ($\gamma = 0.76$) performance. This demonstrates the importance of upstream flow conditioning for overall system effectiveness. Therefore, upstream flow optimization provides cascading benefits throughout the entire DOC-DPF-SCR system, improving overall emission control performance.

ACKNOWLEDGEMENT

This research is financially supported by the Natural Science Foundation of China under the awarded project (NSFC) for International Young Scientists (grant number 51850410521) and the research foundation of the School of Vehicle and Mobility, Tsinghua University in China.

REFERENCES

[1] Peng, Q.; Ye, J.; Kang, Z. (2024). Optimization of diesel oxidation catalyst for enhanced emission reduction in engines, *Energy*, Vol. 290, Paper 130152, 13 pages, doi:10.1016/j.energy.2023.130152

[2] Chen, Z.; Liu, Q.; Liu, H.; Wang, T. (2024). Recent advances in SCR systems of heavy-duty diesel vehicles – low-temperature NOx reduction technology and combination of SCR with remote OBD, *Atmosphere*, Vol. 15, No. 8, Paper 997, 14 pages, doi:10.3390/atmos15080997

[3] Wu, G.; Feng, G.; Li, Y.; Ling, T.; Peng, X.; Su, Z.; Zhao, X. (2024). A review of thermal energy management of diesel exhaust after-treatment systems technology and efficiency enhancement approaches, *Energies*, Vol. 17, No. 3, Paper 584, 32 pages, doi:10.3390/en17030584

[4] Wang, H.; Dang, X.; Huang, Y.; Wang, W.; Yan, D.; Yu, X.; Ren, Y.; Qu, J. (2024). Research progress of Cu-based and Ce-based catalysts for the selective catalytic reduction of NO with CO, *Surfaces and Interfaces*, Vol. 48, Paper 104310, 19 pages, doi:10.1016/j.surfin.2024.104310

[5] Karre, A. V.; Garlapalli, R. K.; Jena, A.; Tripathi, N. (2023). State of the art developments in oxidation performance and deactivation of diesel oxidation catalyst (DOC), *Catalysis Communications*, Vol. 179, Paper 106682, 17 pages, doi:10.1016/j.catcom.2023.106682

[6] Shi, Z.; Peng, Q.; E, J.; Xie, B.; Wei, J.; Yin, R.; Fu, G. (2023). Mechanism, performance and modification methods for NH_3-SCR catalysts: a review, *Fuel*, Vol. 331, Part 2, Paper 125885, 22 pages, doi:10.1016/j.fuel.2022.125885

[7] Zhang, Z.; Tian, J.; Li, J.; Cao, C.; Wang, S.; Lv, J.; Zheng, W.; Tan, D. (2022). The development of diesel oxidation catalysts and the effect of sulfur dioxide on catalysts of metal-based diesel oxidation catalysts: a review, *Fuel Processing Technology*, Vol. 233, Paper 107317, 35 pages, doi:10.1016/j.fuproc.2022.107317

[8] Liao, J.; Hu, J.; Zhong, J.; Yan, F.; Chen, P.; Hu, Y.; Zhu, L. (2022). An experimental investigation of particle and NOx emissions for a non-road diesel engine equipped with an integrated DOC + CDPF + SCR aftertreatment system during different operations, *Environmental Science and Pollution Research*, Vol. 29, No. 42, 63815-63836, doi:10.1007/s11356-022-20152-x

[9] García, A.; Monsalve-Serrano, J.; Lago Sari, R.; Martinez-Boggio, S. (2022). Energy assessment of an electrically heated catalyst in a hybrid RCCI truck, *Energy*, Vol. 238, Part A, Paper 121681, 19 pages, doi:10.1016/j.energy.2021.121681

[10] Belot, I.; Vidal, D.; Greiner, R.; Votsmeier, M.; Hayes, R. E.; Bertrand, F. (2021). Impact of washcoat distribution on the catalytic performance of gasoline particulate filters as predicted by lattice Boltzmann simulations, *Chemical Engineering Journal*, Vol. 406, Paper 127040, 18 pages, doi:10.1016/j.cej.2020.127040

[11] Leskovjan, M.; Němec, J.; Plachá, M.; Kočí, P.; Isoz, M.; Svoboda, M.; Novák, V.; Price, E.; Thompsett, D. (2021). Multiscale modeling and analysis of pressure drop contributions in catalytic filters, *Industrial & Engineering Chemistry Research*, Vol. 60, No. 18, 6512-6524, doi:10.1021/acs.iecr.0c05362

[12] Zhang, X.; Ge, H. E.; Liu, Z.; Liu, Y. Q. (2024). Analysis of flow straightener on the internal flow field of three-phase jet fire monitors, *International Journal of Simulation Modelling*, Vol. 23, No. 1, 101-112, doi:10.2507/IJSIMM23-1-676

[13] Swift, A.; Smoorenburg, E.; Newman, A.; Bogin Jr., G. E. (2023). The impact of environmental conditions on the heat and emissions produced by large diesel engines in underground mines, *Journal of Cleaner Production*, Vol. 429, Paper 139277, 10 pages, doi:10.1016/j.jclepro.2023.139277

[14] Feng, R.; Hu, X.; Li, G.; Sun, Z.; Ye, M.; Deng, B. (2023). Exploration on the emissions and catalytic reactors interactions of a non-road diesel engine through experiment and system level simulation, *Fuel*, Vol. 342, Paper 127746, 11 pages, doi:10.1016/j.fuel.2023.127746

[15] Belot, I.; Vidal, D.; Votsmeier, M.; Hayes, R. E.; Bertrand, F. (2020). Numerical investigation of the impact of washcoat distribution on the filtration performance of gasoline particulate filters, *Chemical Engineering Science*, Vol. 221, Paper 115656, 19 pages, doi:10.1016/j.ces.2020.115656

[16] Granger, P. (2017). Challenges and breakthroughs in post-combustion catalysis: how to match future stringent regulations, *Catalysis Science & Technology*, Vol. 7, No. 22, 5195-5211, doi:10.1039/C7CY00983F

[17] Jung, Y.; Pyo, Y. D.; Jang, J.; Kim, G. C.; Cho, C. P.; Yang, C. (2019). NO, NO_2 and N_2O emissions over a SCR using DOC and DPF systems with Pt reduction, *Chemical Engineering Journal*, Vol. 369, 1059-1067, doi:10.1016/j.cej.2019.03.137

[18] Cumaranatunge, L.; Chiffey, A.; Stetina, J.; McGonigle, K.; Repley, G.; Lee, A.; Chatterjee, S. (2017). A study of the soot combustion efficiency of an SCRF® catalyst vs a CSF during active regeneration, *Emission Control Science and Technology*, Vol. 3, No. 1, 93-104, doi:10.1007/s40825-016-0059-6

[19] Sun, K.; Zhao, H.; Zhao, K.; Li, D.; Bai, S. (2020). Optimization of SCR inflow uniformity based on CFD simulation, *Open Physics*, Vol. 18, No. 1, 1168-1177, doi:10.1515/phys-2020-0221

[20] Wang, Y.; Zhu, Q.; Huang, T.; Han, X.; Lin, M. (2024). Modelling and simulation of nonlinear dynamic flow field and temperature field of depyrogenation tunnel, *Facta Universitatis, Series: Mechanical Engineering*, Vol. 22, No. 1, 45-62, doi:10.22190/FUME221221011W

[21] Yang, X.; Zuo, Q.; Chen, W.; Guan, Q.; Shen, Z.; Li, Q.; Xie, Y. (2023). Improvement of flow field uniformity and temperature field in gasoline engine catalytic converter, *Applied Thermal Engineering*, Vol. 230, Part B, Paper 120792, 14 pages, doi:10.1016/j.applthermaleng.2023.120792

[22] Raghu, M. Y.; Sharma, P. (2017). *Evaluation of performance of DPF cell structure for soot loading, regeneration and pressure drop using CFD simulation*, SAE Technical Paper 2017-26-0111, 8 pages, doi:10.4271/2017-26-0111

[23] Konstandopoulos, A. G.; Kostoglou, M.; Vlachos, N.; Kladopoulou, E. (2005). *Progress in diesel particulate filter simulation*, SAE Technical Paper 2005-01-0946, 31 pages, doi:10.4271/2005-01-0946

[24] Tarbajovsky, P.; Puskar, M.; Sabadka, D. (2023). Simulation model of vehicle emission reduction exhaust system, *International Journal of Simulation Modelling*, Vol. 22, No. 4, 679-689, doi:10.2507/IJSIMM22-4-675